Bull. Inst. Chem. Res., Kyoto Univ., Vol. 62, No. 3, 1984

High Resolution Electron Microscopy of Polymers with Fiber Structure

Ken-ichi KATAYAMA, Seiji ISODA, Masaki TSUJI, Masayoshi OHARA and Akiyoshi KAWAGUCHI*

Received August 2, 1984

The feasibility of electron microscopy was demonstrated for studying the fiber structure of some polymers such as polyethylene [PE], poly (*p*-phenylene terephthalamide) [PPTA] and polymeric sulfur nitride [(SN)x].

The total end point dose (the electron irradiation dose necessary for complete destruction of the crystalline lattice) was measured, and the expected resolution was calculated as about 0.5 nm for PPTA and (SN)x and as about 4.0 nm for PE at 200 keV. Consequently high resolution lattice images of PPTA and (SN)x were expected and really obtained. Thus the fiber structure of PPTA and (SN)x was investigated by comparing the high resolution images and their optical diffractograms with the corresponding dark-field images. For PE fiber whose high resolution images are very difficult to take due to its radiation sensitivity, comparison between dark-field image and strongly defocused bright-field image was useful for studying its fiber structure.

KEY WORDS: Fiber structure/ Polyethylene/ Poly (*p*-phenylene terephthalamide)/ Polymeric sulfur nitride/ Dark-field electron microscopy/ High resolution electron microscopy/

I. INTRODUCTION

Fiber structure has been studied by many researchers to clarify its ultrastructure, that is, the distribution of the crystalline and amorphous regions and the molecular organization in them.[1] Among various methods for this purpose, electron microscopy has a great advantage over others because it can render the local structure visible.[2]

Present-day transmission electron microscopes for high resolution works are so greatly developed that crystal structures can be analyzed directly on an atomic or molecular level, provided that the specimen is resistant enough against electron irradiation.[3] As an application of high resolution electron microscopy to polymer single crystals, several examples of lattice imaging have been reported, notably poly(*p*-xylylene) [PPX],[4,5] and poly[1, 6-di (N-carbazolyl)-2,4-hexadiene] which is one of polydiacetylene.[6] A particularly interesting case is that of PPX single crystals where the direct image of individual molecular chains[5] was used as a successful starting of *X*-ray crystal structure analysis[7] and lattice images including edge dislocations were observed.[8] Furthermore, the fiber structure of some polymers with high resistivity against electron irradiation has begun to be investigated with high resolution electron microscopy : for example, poly(*p*-phenylene terephthalamide) [PPTA][9,10] and poly(*p*-phenylene benzobisthiazole)

* 片山健一, 磯田正二, 辻 正樹, 小原正義, 河口昭義 : Laboratory of Polymer Crystals, Institute for Chemical Research, Kyoto University, Uji, Kyoto-fu 611

[PBT].[11]

The purpose of this paper is to demonstrate the feasibility of electron microscopy for studying the fiber structure of polyethylene [PE], PPTA and polymeric sulfur nitride [(SN)x], by using dark-field imaging and/or high resolution imaging.

II. EXPERIMENTAL

PE fiber[12] for electron microscopic observation was prepared by hot drawing of Sholex 6050 film cast on the hot water surface from a solution in *p*-xylene and subsequent annealing at 127°C.

PPTA sample used was Kevlar which is a commercial product by Du Pont, and (SN)x sample was kindly provided by Prof. Nakata, University of Tokyo. Fibrillar fragments of PPTA were obtained by tearing off the specimen at room temperature after annealing at 400°C and those of (SN)x were obtained by crushing the specimen to fine pieces at liquid nitrogen temperature.

Electron microscopic observations were carried out with JEM-200CS. Radiation damage for several polymers was measured by observing the changes of selected area diffraction patterns due to electron bombardment.

III. RESULTS AND DISCUSSION

The total end point dose (*i.e.*, the electron irradiation dose necessary for complete disappearance of all crystalline reflections in the diffraction pattern) was measured for PE, PPTA and (SN)x. The results were shown in Table I together with the expected resolution, d [nm], calculated by the modified Rose equation,[13,14]

$$d = 1/50C\sqrt{fQ}, \qquad (1)$$

where C is the contrast, f the net utilization factor, and Q the total end point dose on specimen in units of Coulomb/cm^2. The d-values in Table I are calculated assuming $f=0.25$ and $C=0.1$. PPTA and (SN)x are much more durable against electron irradiation than PE. The d-values for PPTA and (SN)x are around 0.5 nm and corresponding to the most stable lattice spacings of them ((110) spacing for PPTA and $(\bar{1}02)$ for (SN)x). Thus lattice imaging of PPTA and (SN)x whose morphologies are originally fibrillar can be expected and have been realized. Therefore the fiber structure of them can be discussed by comparing their high resolution images with the corresponding dark-field images. The d-value of PE is rather large, 4.0 nm, and no lattice image of PE has been reported. Here we will discuss the fiber structure of

Table I Total end point dose Q and expected resolution d

Polymer	Q [Coulomb/cm^2]	Electron energy [keV]	d[nm]
PE*	0.01	200	4.0
PPTA**	0.4–0.8	200	0.6–0.4
(SN)x**	0.5–0.8	200	0.5–0.4

* single crystal, ** fiber

PE on the basis of its dark-field and strongly defocused bright-field images.

1. PE fiber

Figure 1-a shows a selected-area electron diffraction pattern and Fig. 1-b a dark-field image of PE taken with 110 and 200 reflections. The locations of all crystallites which are properly oriented to give 110 or 200 reflection should be seen in the dark-field image. Figure 1-b clearly shows that the fiber is made up of small crystallites (bright spots in the dark background) whose longitudinal thickness and lateral dimension are about 20 nm. It should be noted that bright spots align in the vertical direction. That is to say, the crystallites tend to align along the fiber axis, which suggests the existence of microfibrils with their lateral width of several tens of nm.[15]

Another useful method to study the fiber structure of PE is the bright-field defocus imaging.[16] Since the contrast in defocus imaging is caused by the variation of inner potential in the specimen, the distribution of the amorphous and crystalline regions is expected to be visualized. In this case, the optimum value of the defocus, Δf ($\Delta f > 0$ for underfocus), required to give maximum phase contrast for a particular spacing r (>1 nm) in the specimen can be estimated from the following equation:[17]

$$\Delta f = \pm r^2/2\lambda \qquad (2)$$

where λ is the electron wave length. For example, at 200 KV ($\lambda = 0.00251$ nm), the value of Δf for $r = 10$ nm is calculated as about 20 μm underfocus or overfocus.

Figure 2-a taken with this method (at underfocus around the magnitude calculated above) clearly shows a wavy stacking of lamellae as dark bands running in the horizontal direction. Bright bands with about 10 nm in vertical thickness correspond to the amorphous region between crystalline lamellae. The lateral dimension of these lamellae is of the order of μm and much larger than that of the crystallites shown as

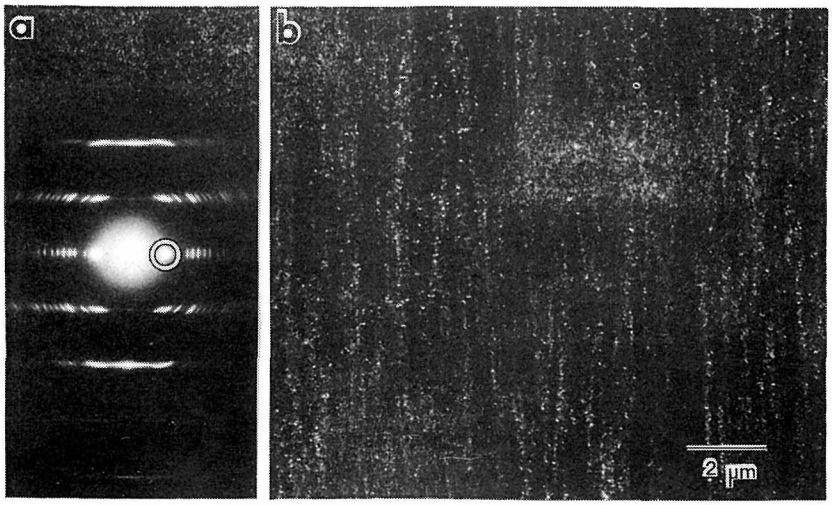

Fig. 1. (a) : Electron diffraction pattern of drawn PE film where the fiber axis is vertical. White circle represents the position of the objective aperture to take dark-field image (b).
(b) : Dark-field image taken with 110 and 200 reflections.

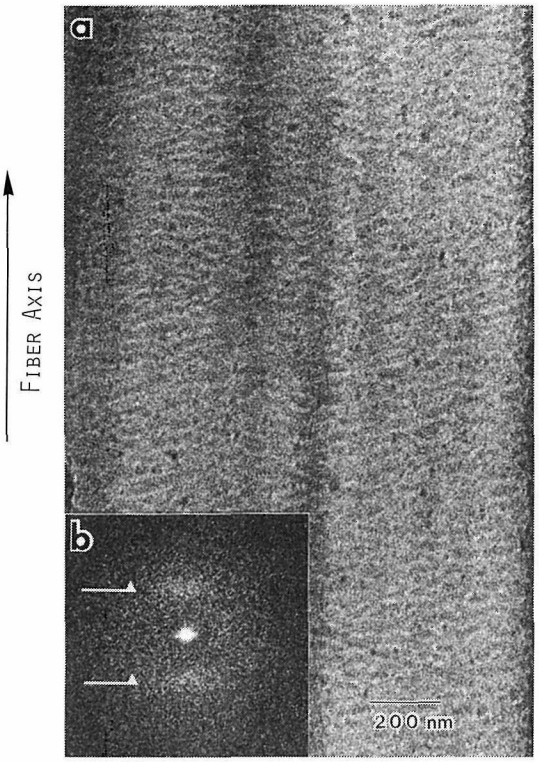

Fig. 2 (a) : Strongly defocused bright-field image of drawn PE film. The fiber axis is vertical.
(b) : Optical diffractogram of (a), which corresponds to the small angle scattering pattern from the specimen. White arrows indicate the diffaction intensity-maxima.

bright spots in Fig. 1-b, whereas the thickness of the lamellae is the similar magnitude to that of the crystallites. This fact suggests that a lamella is composed of many crystallites which do not have the same orientation, that is, a lamella has the mosaic texture. The optical transform (Fig. 2-b) of the image (Fig. 2-a) has broad but apparent intensity-maxima which are indicated by arrows. It reveals the existence of periodic texture consisting of stacked lamellae, corresponding to the small angle *X*-ray scattering (SAXS) pattern from the PE fiber.

A structure model of the PE fiber is shown in Fig. 3, based on the information from both dark-field and defocus images. Part A in the figure indicates the amorphous region and part C a crystalline region which is properly oriented to give 110 or 200 reflection in the electron diffraction pattern for a given incident beam direction. The crystallites of part C align along the fiber axis, *i. e.*, microfibrillar structure. Part C′ is also a crystalline region, but it does not satisfy the Bragg condition for either of the two reflections in question, 110 and 200.

2. PPTA fiber

A dark-field image of PPTA taken with 006 reflection is shown in Fig. 4-b. It

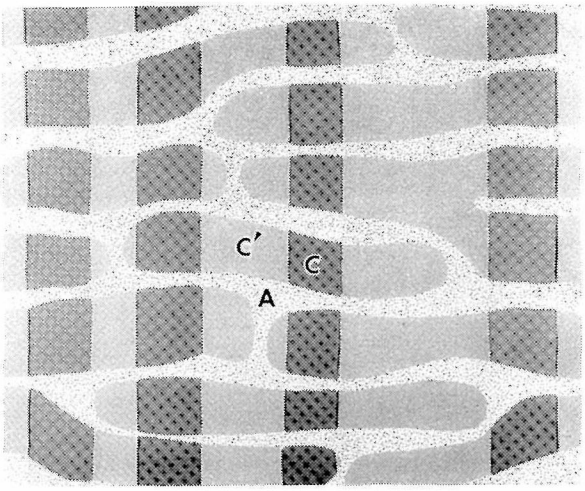

Fig. 3. Structural model for PE fiber.

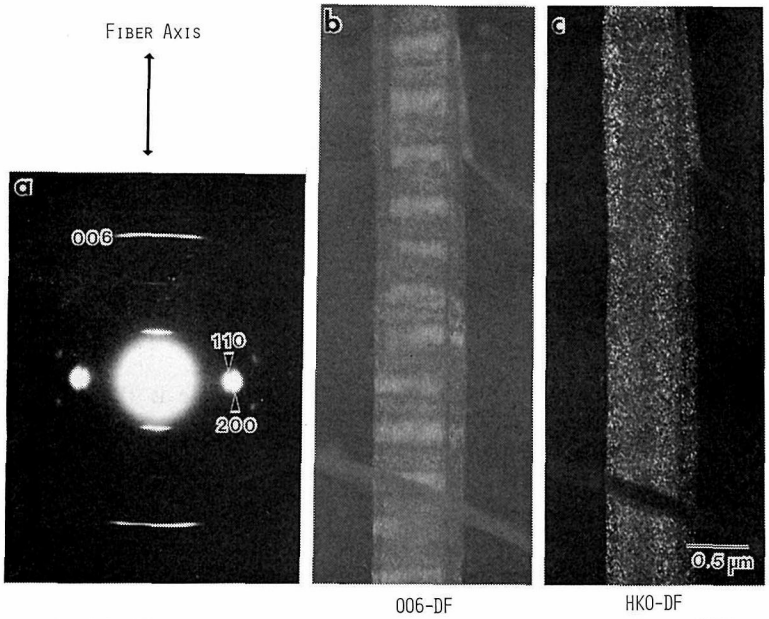

Fig. 4. (a) : Electron diffraction pattern of PPTA fiber annealed at 400°C.
(b) : 006 dark-field image of PPTA.
(c) : 110 and 200 dark-field image of the same specimen-portion that was used for (b).

shows a periodical banded texture which consists of alternating bright and dark bands with the period of about 500 nm, as reported in longitudinal thin sections[10,18] and in the fibrillar fragments[19]. Inspection of the figure shows that there exist microfibrils running along the fiber axis and through these bands. Though Takahashi *et al.*[19] has observed a line of bright spots in a bright band of the 006 dark-field image, this is not recognized in Fig. 4-b. The difference between their results and ours might be due to

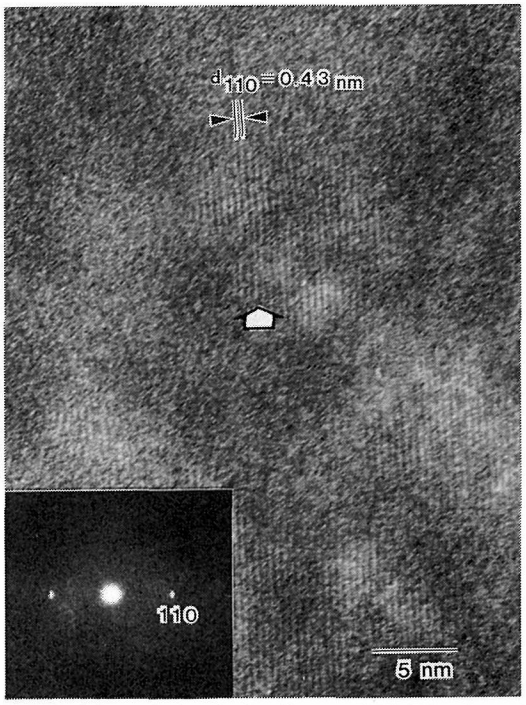

Fig. 5. High resolution lattice image of PPTA. Inset is the optical diffractogram of the image.

the sample preparation: they used the axially compressed fiber of PPTA.

Figure 4-c is a dark-field image taken with 110 and 200 reflections of the same specimen-portion that was used in Fig. 4-b. This figure reveals that small crystallites (bright spots in the figure) are randomly dispersed throughout the fibrillar ribbon[10,19]. By careful inspection of the figure, bright spots seem to be placed in a row in a certain region of the ribbon. A high resolution lattice image of the PPTA fiber is shown in Fig. 5. Clear (110) lattice fringes can be seen. The area where lattice fringes appeared is of the order of 10 nm × 10 nm through 20 nm × 20 nm, and almost the same order as the area of a bright spot which appeared in Fig. 4-c. In the case of PBT fiber, such an area is slightly larger than that of PPTA and 20 nm wide by 40 nm long in the fiber axis.[11] This seems to suggest the reason PBT fiber has a higher modulus than PPTA fiber. The directon of the (110) fringes in Fig. 5, that is the *c*-axis of each crystallite, fluctuates slightly relative to the fiber axis in the plane of the figure. Even curved fringes can sometimes be seen within an area where lattice fringes appear.[10] An example of curved fringes is easily recognized by inspection in the direction indicated by the arrow in Fig. 5. This means the local distortion of (110) lattice planes in the PPTA crystallites.

Since PPTA is made of rigid macromolecules, it cannot have the two-phase structure prevailing in flexible macromolecules such as PE, but has a microfibrillar texture which is similar to a model of bundling of parallel microfibrils proposed by Peterlin.[20] In fact, the SAXS shows no discrete maxima,[10] suggesting a single-phase structure.

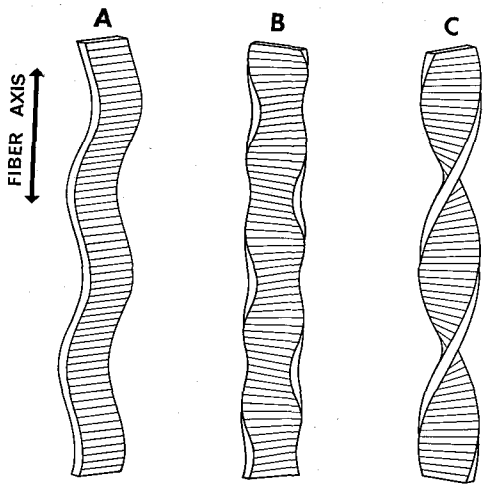

Fig. 6. *Some types of distortion of a microfibril in a well-oriented fiber.*
Model A : Periodic bending,
Model B : Alternate twisting,
Model C : Herical twisting.

The curved (110) fringes in lattice images and the results of dark-field imaging with 006 reflection or 110 and 200 reflections suggest that the microfibrils are distorted by bending and/or twisting. Figure 6 shows some types of distortion of a microfibril in a well-oriented fiber. Model A illustrates the periodic bending, Model B the alternate twisting, and Model C the herical twisting. The twisting (B and C) can be detected in the dark-field image taken with hk0 reflection, whereas the periodic bending can be detected by 00*l* dark-field imaging. Thus the 006 dark-field image of PPTA (Fig. 4-b) reveals that individual microfibrils in a fibrillar ribbon have the same texture of periodic bending, and as the consequence the ribbon possesses a pleated sheet texture.[18] The 110 and 200 dark-field imaging, however, reveals the existence of the twisting of microfibrils in the same ribbon (see Fig. 4-c). Therefore, it should be concluded that a microfibril in PPTA fiber is bending along its fiber axis with rather large periodicity (about 500 nm) as illustrated in Fig. 6-A, and also twisted around the axis. The bending angle is not so large but a few degrees at the most.[18] A periodic banded structure (*i.e.*, periodic bending of a microfibril) has, however, never been observed in fibers of the Kevlar family with the highest modulus (*e.g.* PRD 49).[10,18]

3. (SN)x fiber

Polymeric sulfur nitride (SN)x is well known for its behaviour as a superconductor at low temperatures. Figure 7-b shows a dark-field image of (SN)x fiber taken with 002 and $\bar{1}02$ reflections and Fig. 7-c with 020 reflection.[21] Fine striations are recognized along the chain direction (b-axis, vertical) in Fig. 7-b and these correspond to the microfibrils in which the (002) or ($\bar{1}02$) lattice plane is oriented to satisfy the Bragg condition. A coherent domain (microfibril) is very long along the chain axis, but very narrow in the lateral dimension.[22] Therefore, a microfibril in (SN)x fiber is untwisted

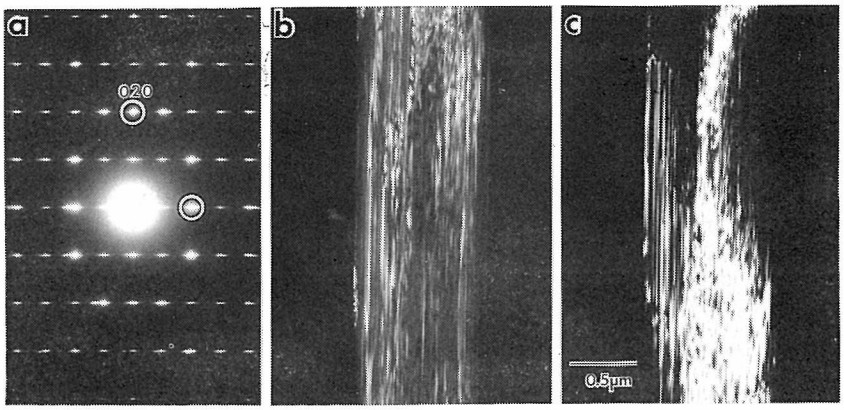

Fig. 7. (a) : Electron diffraction pattern of (SN)x fibril. White circles represent the positions of the objective aperture to take respective dark-field images.
(b) : Dark-field image taken with 002 and $\bar{1}02$ reflections.
(c) : 020 dark-field image of the same specimen-portion that was used for (b).

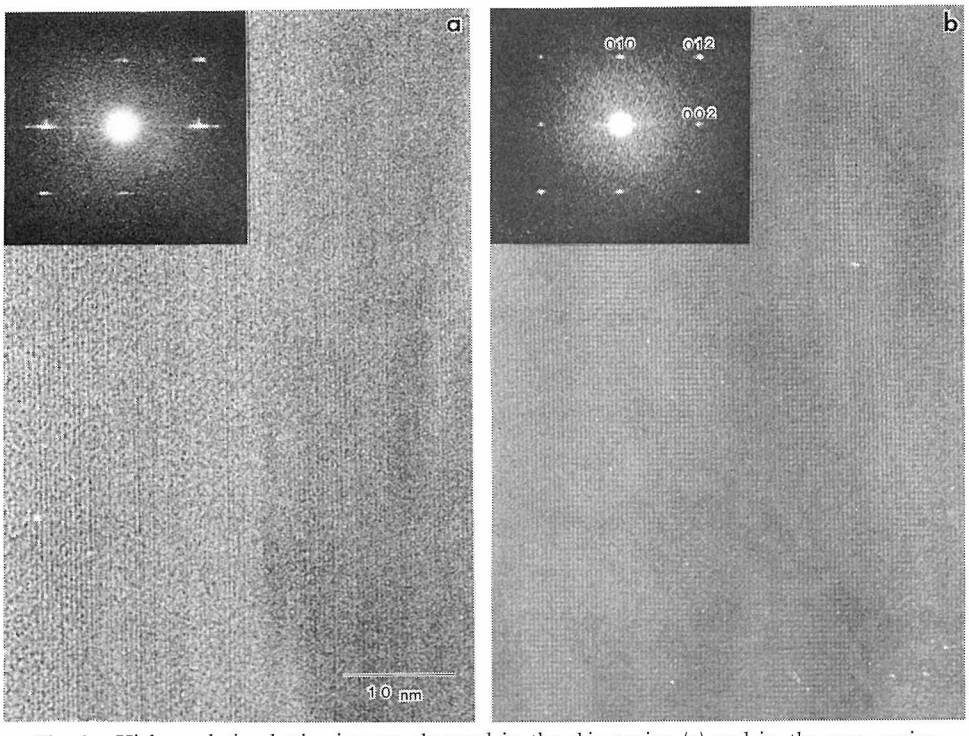

Fig. 8. High resolution lattice images observed in the skin region (a) and in the core region (b) of (SN)x. Insets are the optical diffractograms of the respective images.

and distinct from that in PPTA fiber. Such microfibrillar texture can be also deduced from the electron diffraction pattern (Fig. 7-a), where each reflection streaks in the direction perpendicular to the fiber axis.

Figure 8 shows high resolution lattice images of (SN)x. In the image of the (SN)x

skin region of a fibrillar fragment, (002) lattice fringes (0.359 nm in spacing) are observed (Fig. 8-a). The lateral width of the domain where the fringes appeared is small and only about 2 nm. On the other hand, the core region gives a high resolution image of the single-crystal-like domain where (002) and (010) fringes (0.44 nm in spacing) are particularly well observed. The lateral dimension of the coherent domain is much larger than that in the skin region. This can be also deduced by comparison of the optical diffraction patterns inserted in Figs. 8-a and 8-b.

IV. CONCLUDING REMARKS

In PE, the stacking of lamellae causing the SAXS is observed by bright-field defocus imaging (Fig. 2). That has also been observed by chlorosulphonation and subsequent negative-staining,[23] but it should be noted that this method is useful only for PE, unlike defocus imaging. Moreover, the dark-field imaging of PE reveals that a lamella consists of many crystallites, and the microfibrillar structure is also observed at the same time (Fig. 1). For PPTA, the lamellar texture is not observed, as expected from the nature of the molecules. The crystallite size in PPTA is very small (Fig. 4-c) and the c-axis of the crystallite is slightly disoriented with respect to the fiber axis (Fig. 5). In (SN)x, the crystallite is quite large in length along the chain axis (b-axis) and very small in the lateral direction in shape, and the chain direction in the crystallite is exactly oriented along the fiber axis (Fig. 7 and 8).

Electron microscopy, especially high resolution electron microscopy reveals the ultrastructure of fibers which varies from specimen to specimen, as demonstrated in this paper. Recently in microfibrils of *Valonia* cellulose[24] and in single crystals of isotactic polystyrene,[25] both of which are much more radiation-sensitive than PPTA and (SN)x, direct lattice imaging has been achieved with a special equipment for low dose imaging. By using the equipment, the electron dosage that the specimen will receive can be minimized to the level only necessary for the image recording itself.[26] High resolution imaging will be expected with this technique for studying the fiber structure of rather radiation-sensitive polymers.

REFERENCES AND NOTE

(1) For examples, "Applied Fibre Science", Vol. 1 (1978), Vols. 2 & 3 (1979), Ed. by F. Happey, Academic Press, London.
(2) "Zusetu : Sen-i no Keitai (Morphology of Fibers)" (in Japanese), Ed. by H. Kawai and T. Tagawa, Asakura, Tokyo (1982).
(3) Proc. 47-th Nobel Symp., Lidingö (1979), "Direct Imaging of Atoms in Crystals and Molecules", Ed. by L. Kihlborg, Royal Swedish Academy of Sciences, Stockholm ; Chemica Scripta, **14**, (1978/79).
(4) G. A. Bassett and A. Keller ; cited by A. Keller, *Kolloid-z.*, **231**, 386 (1969).
(5) M. Tsuji, S. Isoda, M. Ohara, A. Kawaguchi and K. Katayama, *Polymer*, **23**, 1568 (1982).
(6) R. T. Read and R. J. Young, *J. Mater. Sci.*, **16**, 2922 (1981).
(7) S. Isoda, M. Tsuji, M. Ohara, A. Kawaguchi and K. Katayama, *Polymer*, **24**,1155 (1983).
(8) S. Isoda, M. Tsuji, M. Ohara, A. Kawaguchi and K. Katayama, *Makromol. Chem. Rapid Commun.*, **4**, 141 (1983).
(9) M. G. Dobb, A. M. Hindeleh, D. J. Johnson and B. P. Saville, *Nature*, **253**, 189 (1975).

(10) M. G. Dobb, D. J. Johnson and B. P. Saville, *J. Polym. Sci. Polym Symp.*, **58**, 237 (1977).
(11) K. Shimamura, J. R. Minter and E. L. Thomas, *J. Mater. Sci. Letters*, **2**, 54 (1983).
(12) The word "fiber" is used in a broad sense for a specimen with fibrillar structure.
(13) R. M. Glaeser, Proc. 3-rd Int, Conf. HVEM, Oxford, 370 (1974).
(14) I. A. Kuo and R. M. Glaeser, *Ultramicrosc.*, **1**, 53 (1975).
(15) K. Sakaoku and A. Peterlin, *Makromol. Chem.*, **108**, 234 (1967).
(16) J. Petermann and H. Gleiter, *Phil. Mag.*, **31**, 929 (1975).
(17) D. J. Johnson and D. Crawford, *J. Microsc.*, **98**, 313 (1973).
(18) M. G. Dobb, D. J. Johnson and B. P. Saville, *J. Polym. Sci. Polym. Phys. Ed.*, **15**, 2201 (1977).
(19) T. Takahashi, M. Miura and K. Sakurai, *J. Appl. Polym. Sci.*, **28**, 579 (1983).
(20) A. Peterlin, *J. Macromol. Sci.-Phys.*, **B8**, 83 (1973).
(21) M. J. Cohen, A. F. Garito, A. J. Heeger, A. G. MacDiarmid, C. M.Mikulski, M. S. Saran and J. Kleppinger, *J. Amer. Chem. Soc.*, **23**, 3844 (1976).
(22) W. D. Gill, W. Bludau, R. H. Geiss, P. M. Grant, R. L. Greene, J. J. Mayerle and G. B.Street, *Phys. Rev. Letter*, **38**, 1305 (1977).
(23) G. Kanig, *Kolloid-z.*, **251**, 782 (1973).
(24) J. Sugiyama, H. Harada, Y. Fujiyoshi and N. Uyeda, *Mokuzai Gakkaishi*, **30**, 98 (1984).
(25) M. Tsuji, S. K. Roy and R. St. J. Manley, *Polym. Commun.*, in press.
(26) Y. Fujiyoshi, T. Kobayashi, K. Ishizuka, N. Uyeda, Y. Ishida and Y. Harada, *Ultramicrosc.*, **5**, 459 (1980).